CHALMERS
UNIVERSITY OF TECHNOLOGY

Development of a novel numerical framework in OpenFOAM to simulate Kaplan turbine transients

Development of a novel numerical framework in OpenFOAM to simulate Kaplan turbine transients

Saeed Salehi[1], Håkan Nilsson[1], Eric Lillberg[2] and Nicolas Edh[2]

[1] Chalmers University of Technology, Gothenburg, Sweden
[2] Vattenfall AB, Stockholm, Sweden

E-mail: saeed.salehi@chalmers.se

Abstract.

A novel numerical framework in OpenFOAM is proposed in this work, to simulate transient operation of Kaplan hydraulic turbines. Such transient operations involve a variation of both runner blade and guide vane angles, which also gives rise to a flow rate variation. A numerical simulation of such a process is very challenging, since it requires a deformation of both guide vane and runner meshes, with mesh slip conditions at arbitrarily shaped surfaces, at the same time that the runner mesh is rotating around the turbine axis. The currently available mesh morphing methodologies in OpenFOAM are not able to properly accomplish this. Thus a novel framework for OpenFOAM, including dynamic mesh solvers and boundary conditions, is developed to tackle this problem.

The new framework is utilized to simulate the flow during transient operation of the U9-400 Kaplan turbine model. The guide vanes and runner blades are rotated individually around their own axes with a constant rotational speed, while the runner is rotating, and the flow rate is linearly changed with the guide vane angle. It is shown that the novel numerical framework can successfully be utilized to simulate the load change of Kaplan turbines.

1. Introduction

Renewable electric energy resources, such as solar and wind have been rapidly growing in recent years. These resources are not always available and may vary even during day time [1]. Due to the fast growth of intermittent resources, hydraulic turbines are operated in transient, variable load, conditions to regulate the electrical grid. Hydraulic turbines are generally designed to continuously work at the best efficiency condition. Transient operation causes additional stresses on the turbines, and reduces their lifetime. Therefore, it is essential to develop methodologies to study the details of the flow under such conditions. The transient operation of Kaplan turbines involves a change of flow rate, change of guide vane angles, and change of runner blade angles while the runner is rotating. Hence, the numerical simulation of such transients can be tremendously challenging.

In the present work, a numerical framework is developed in the OpenFOAM open-source CFD package to simulate transients in Kaplan turbines. A large number of code developments were carried out to establish the required numerical framework. The presently available explicit slip correction boundary condition does not work appropriately for large mesh deformations at curved surfaces. As a remedy, a method is proposed and implemented in OpenFOAM to make

the points smoothly slip on the curved surfaces of Kaplan turbines. A special methodology is needed when the mesh is rotating at the same time as it is deforming, as is the case for Kaplan turbine runners. Special care must be taken for the runner blades, since their axes are rotating with the runner rotation.

The numerical framework is utilized to simulate the flow in the U9-400 Kaplan turbine model, going from an operating condition close to the best efficiency point to a part load condition. The guide vanes and runner blades are rotated around their own axes with a constant rotational speed, and the flow rate is linearly changed with the guide vane angle. The numerical results are used for studying the flow behavior, such as the formation of the rotating vortex rope and the frequencies that occur in the system.

2. Developed numerical framework

Transient operation of Kaplan turbines involves a variation of both guide vane and runner blade angles at the same time as the runner is rotating around the turbine axis. From a numerical point of view, different types of mesh motion are needed in the computational domain. The mesh motion of the runner domain consists of simultaneous solid-body rotation and mesh morphing, while the guide vane mesh motion includes only mesh deformation due to morphing. Each guide vane and runner blade changes its angle about its own axis, and the runner blade axes also have the solid-body rotation of the runner. While the mesh is deformed, it must slip on arbitrarily shaped surfaces, such as the hub and the shroud, and in some cases even on the blades. This makes the mesh morphing procedure more difficult. Thus, simulations of the flow in Kaplan turbines during transient operation is very challenging and needs special developments that are described in the current section.

2.1. Novel mesh morphing approach

The original mesh morphing approach in OpenFOAM solves a Laplacian equation to diffuse the boundary mesh deformation through the computational domain. The governing equation, given by

$$\nabla \cdot (k \nabla \boldsymbol{\delta}_{\text{cell}}) = \mathbf{0}, \tag{1}$$

is solved for each time step, where k is the mesh motion diffusivity and $\boldsymbol{\delta}_{\text{cell}}$ is the displacement vector of the cell centers (i.e., `cellDisplacement`). The displacement vector of the mesh points, $\boldsymbol{\delta}_{\text{point}}$ (i.e., `pointDisplacement`), used for the actual deformation of the mesh, is obtained using linear interpolation from the cell displacement. Consequently, in each time step, the location of the new point positions are calculated by

$$\boldsymbol{x}^{\text{new}}_{\text{point}} = \boldsymbol{x}^{\text{old}}_{\text{point}} + \boldsymbol{\delta}_{\text{point}}. \tag{2}$$

In this approach, although the Laplacian equation is solved for the $\boldsymbol{\delta}_{\text{cell}}$ field, one can impose the boundary conditions on the $\boldsymbol{\delta}_{\text{point}}$ field and OpenFOAM automatically calculates the corresponding boundary conditions of the $\boldsymbol{\delta}_{\text{cell}}$ field. Let us consider the runner domain, in which a Dirichlet (fixed value) boundary condition is applied on the `pointDisplacement` field of the runner blade to prescribe its change in blade angle. This Dirichlet boundary condition handles the rotation of each runner blade around its own axis using a prescribed rotational speed which changes through time. The points on the inlet and outlet boundaries of the runner are also fixed using a zero displacement Dirichlet boundary condition. In order to have a smooth mesh deformation, the points on the hub and shroud boundaries should be able to slip on their corresponding curved surfaces. A slip boundary condition calculates the quantity of interest (here `pointDisplacement` field) through a zero-gradient assumption and then removes the normal component of this quantity with respect to the boundary surface. In other words,

only tangential components is kept, using

$$\boldsymbol{\delta}_{\parallel} = \boldsymbol{\delta} - (\boldsymbol{\delta} \cdot \hat{n}) \cdot \hat{n}, \tag{3}$$

where $\boldsymbol{\delta}_{\parallel}$ is the tangential component of the displacement vector (point or cell) and $\hat{n}$ is the unit normal vector to the boundary surface. It is obvious that a general slip boundary condition does not have an implicit implementation that contributes to the coefficient matrix. Instead, it works as an explicit correction.

This explicit implementation may work fine for small mesh deformations or for surfaces with small curvatures, but it cannot handle large deformations or highly curved surfaces. Slip boundary conditions based on the classical explicit correction are shown to have severe convergence issues on complex geometries [2]. For this reason, in the current study, a novel methodology is developed in OpenFOAM to treat surface slip displacements in a more robust way. The main idea is to have two different displacement fields and solve the Laplacian equation for each of those fields. The first Laplacian solution gives an intermediate displacement field $\boldsymbol{\delta}_0$ in which a conventional explicit surface slip displacement boundary condition is used to slip points on the curved surfaces. Then the tangential component of the intermediate displacement field is computed and set as a Dirichlet boundary condition for the main displacement field $\boldsymbol{\delta}$. In this way, the points inside the domain *feel* the slip boundary surface and move with the same curvature. A new mesh motion solver is developed in OpenFOAM and the above-described methodology is implemented. In addition, a new boundary condition is implemented to extract the tangential component of $\boldsymbol{\delta}_0$ on the slipped surface and to apply it as a Dirichlet boundary type for the $\boldsymbol{\delta}$ field.

2.2. Simultaneous solid body rotation and deformation

The runner blade angles change while the whole runner is rotating around the turbine axis. Accordingly, the mesh motion of the runner domain includes both solid-body rotation and mesh morphing. A new mesh motion solver is developed in OpenFOAM to handle such a mesh motion. In each time step, the solver first morphs the mesh employing the methodology described in Section 2.1 to diffuse the mesh deformation due to change in the runner blade angle. Subsequently, it applies a solid body transformation (here a rotation around turbine axis) on the morphed mesh. It should be noted that the mesh deformation calculation is always performed in to the original runner position.

2.3. Correction of point locations

A new dynamic mesh class is developed to make sure that slipped points on the curved surfaces (runner hub and shroud and guide vane lower and upper surfaces) follow the exact mathematical equation of those surfaces. The equations are extracted from the geometry of the turbine and provided inside the dynamic mesh class. This correction step is performed as the final mesh step in updating the mesh at each time step. To put it another way, first, the location of each point is calculated through the procedure described in Sections 2.1 and 2.2 and then just before updating the mesh, the location of the points are corrected. The mesh quality parameters were monitored throughout the transient operation.

3. Case study

3.1. U9-400 model turbine

A new Kaplan turbine model called U9-400 was chosen as the case study in this investigation. The "400" in the name indicates the diameter of the runner in mm. The test case is a 1:3.875 scale model of the hydropower plant Porjus U9 prototype which is located in the north of Sweden. The model scale experimental setup is being constructed at Vattenfall Research and

Development in Älvkarleby. It is a down-scaled version of a previously investigated U9 model, for upcoming studies of transient operation. All the previously published researches on this test case (e.g., [3, 4, 5, 6]) studied the the old larger turbine model with runner diameter of 500 mm.

A three-dimensional view of the U9-400 model turbine is presented in Figure 1. The model is assembled with a spiral casing, 18 stay vanes, 20 guide vanes, a runner, and draft tube. The diameter of the runner is $D = 0.4$ m and consists of 6 runner blades. The best efficiency point (BEP) for this down-scaled model is yet to be determined. In the present work a BEP* (asterisk because it is approximate) is determined from the previous model tests, and given by the following. The guide vanes and runner blades are at the opening of 26° and 32.8°, measured from the fully closed position (blades touching each other). It has a head of $H = 6.97$ m, a flow rate of $Q = 0.426$ m^3/s, and a runner rotational speed of $\omega = 839$ rpm.

Figure 1: U9-400 model turbine assembly

3.2. Transient operation sequence

The experimental conditions are yet to be determined. Thus, in the present work a load rejection sequence from BEP* to Part Load (PL) is designed to assess the novel numerical framework for studies of transients in Kaplan turbines. The runner blade and guide vane angles are reduced by 4° and 6°, respectively, during 2 s. The prescribed turbine flow rate is assumed to change linearly with the guide vane angle. The variation of blade angles and volume flow rate are shown in Figure 2. The turbine operates at steady BEP* and PL conditions during 2 s before and after the transient, respectively

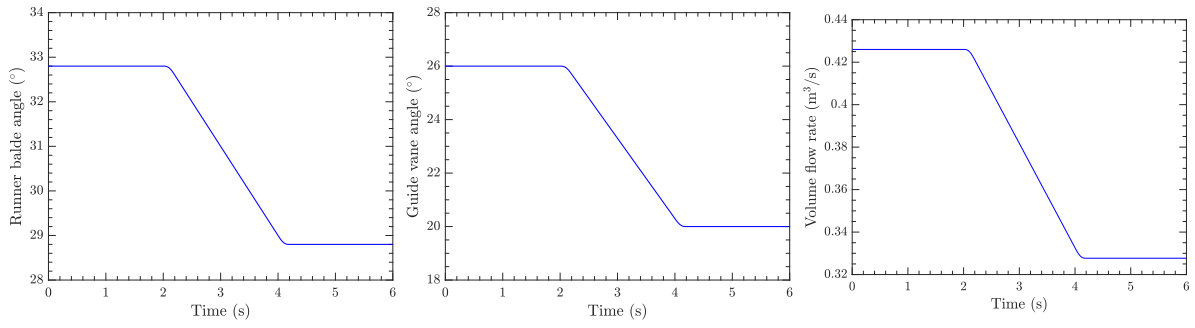

(a) (b) (c)

Figure 2: Variation of the (a) runner blade angle, (b) guide vane angle, and (c) volume flow rate for the load rejection sequence.

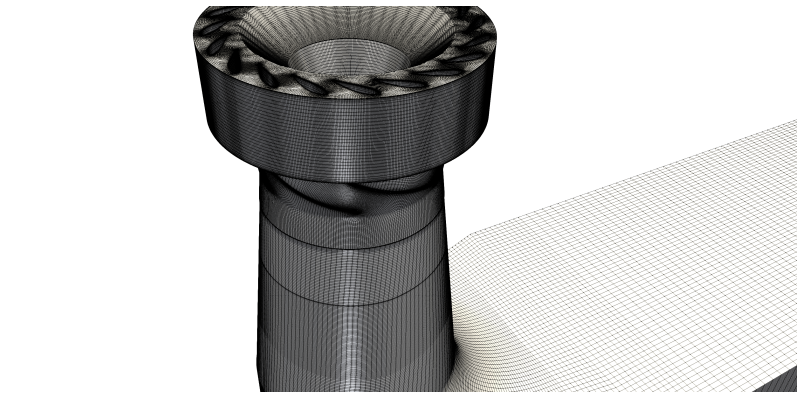

(a) Assembly

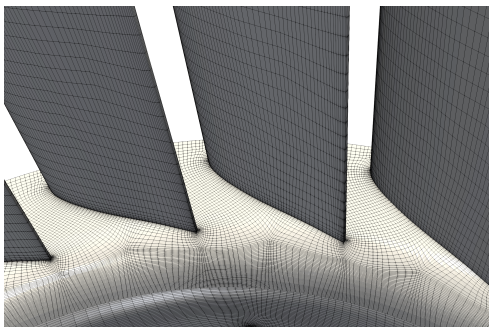

(b) Guide vanes

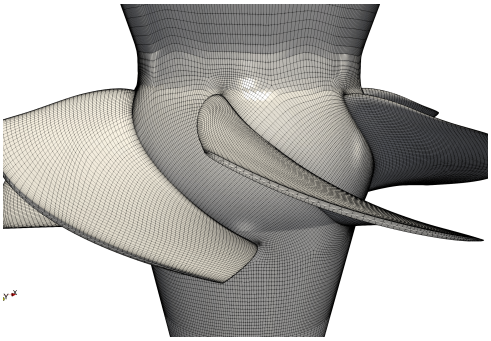

(c) Runner

Figure 3: Computational mesh at BEP*

3.3. Computational details

The spiral casing and stay vanes are not considered in this study, and the computational domain starts at the guide vane inlet and ends at the draft tube outlet. This computational domain includes everything that is necessary to assess the novel numerical framework for studies of transients in Kaplan turbines. Figure 3 shows different views of the computational mesh at the BEP* condition, before morphing the mesh. The guide vane and runner grids are generated in ANSYS Turbo-Grid, whereas ANSYS ICEM-CFD is utilized to generate the draft tube mesh. The guide vane, runner, and draft tube domains contain 2.7×10^6, 2.1×10^6, and 3.4×10^6 hexahedral cells, respectively.

The computations are carried out using OpenFOAM-v1912. The turbulence is modelled using the $k-\omega$ SST SAS model [7]. The temporal derivatives are discretized using the implicit second-order backward scheme. The divergence (convective) terms in the momentum equation are discretized using the Linear-Upwind Stabilised Transport (LUST) scheme [8].

The pressure-velocity coupling is conducted through the PIMPLE algorithm, which combines the SIMPLE [9] and PISO [10] algorithms. PIMPLE applies the SIMPLE correction as an outer loop of the inner PISO correction. A maximum of 10 outer loops and 2 inner loops are performed in each time step. One additional non-orthogonal correction is also carried out in each inner loop to ensure convergence of all explicit parts in the discretized equations, such as the non-orthogonal correction term.

Figure 4 shows a flow chart of the computation procedure, including the novel dynamic mesh framework and the PIMPLE algorithm. The mesh motion calculations are performed at the beginning of the first outer correction in the PIMPLE loop.

The radial and tangential components of the inlet velocity are imposed using a time-varying

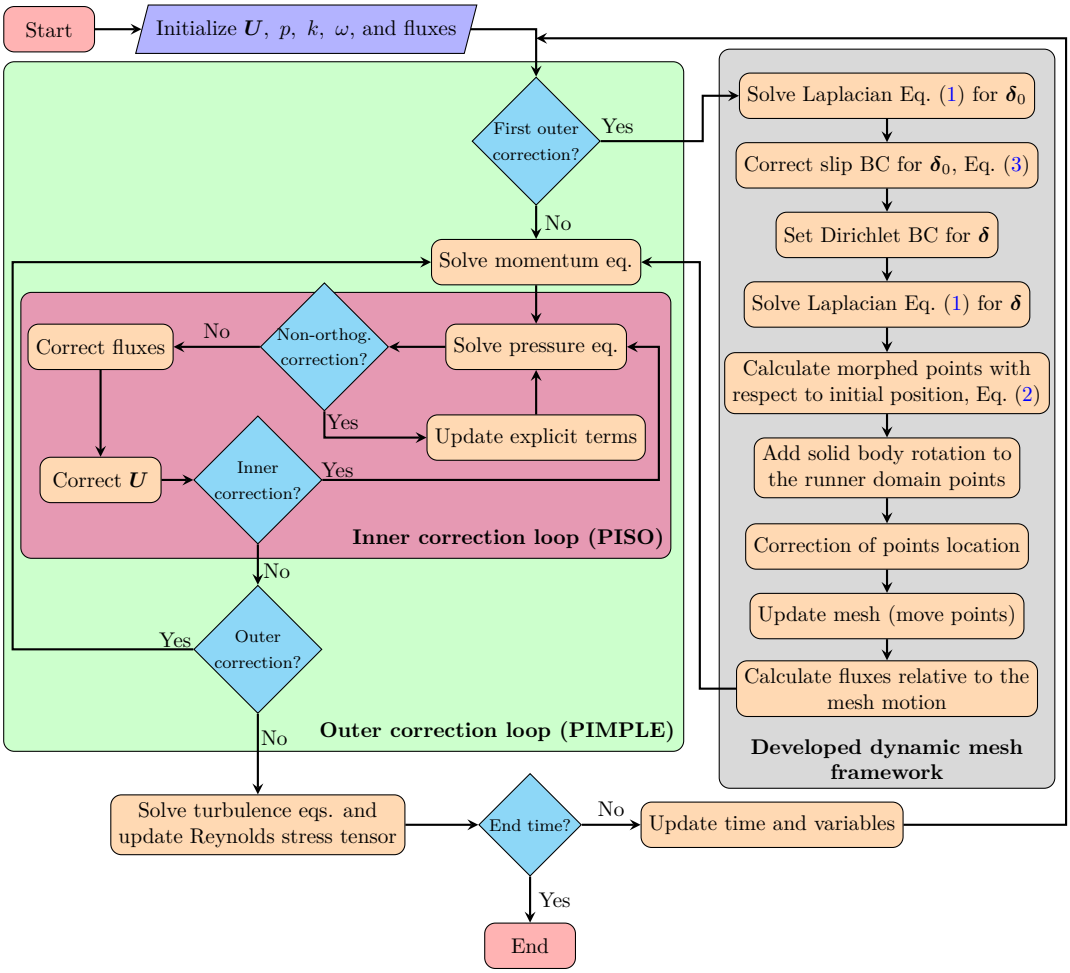

Figure 4: Flow chart of the computational procedure, showing the implementation of the novel dynamic mesh framework inside the OpenFOAM PIMPLE algorithm

boundary condition according to the volume flow rate variation in Figure 2c, keeping the flow direction aligned with the stay vane trailing edges. In other words, it is assumed that the stay vanes (not part of the computational domain) ideally guide the flow. The k and ω values at the inlet are computed using a fixed turbulence intensity $I = 7\%$ and viscosity ratio $\nu_t/\nu = 100$. A zero-gradient condition is applied for the pressure at the inlet boundary, while a constant pressure condition is applied at the outlet boundary. A zero-gradient condition is imposed for all other variables at the outlet boundary. The `cyclicAMI` coupling boundary condition is employed between the rotating (runner) and non-rotating regions (guide vanes and draft tube).

4. Results and discussion

The novel numerical framework is adopted to simulate a load rejection procedure of the U9-400 turbine model, and the results are presented and discussed in this section. As previously shown in Figure 2, the transient operation sequence starts with a constant operation at the BEP* condition ($t = 0 \rightarrow 2$ s), followed by a load rejection ($t = 2 \rightarrow 4$ s), reaching the PL condition where it stays at constant operation ($t = 4 \rightarrow 6$ s). Before this procedure, the flow field is simulated for 3 s to make sure that a statistically stationary state is reached.

The computational meshes of the guide vane and runner domains are shown in Figure 5

(unmorphed at BEP* and morphed at PL) . The meshes are colored with the magnitude of the cell displacement, to show how far the cell centers have been moved due to the morphing. It is seen that the maximum displacement occurs close to the leading and trailing edges of the guide vanes and runner blades, since those cells are close to the boundary that is being rotated, and furthest away from the center of rotation. The diffusion of the mesh motion further away from those boundaries is influenced by the diffusivity coefficient, which in the present case is calculated using the inverse distance from the moving boundaries.

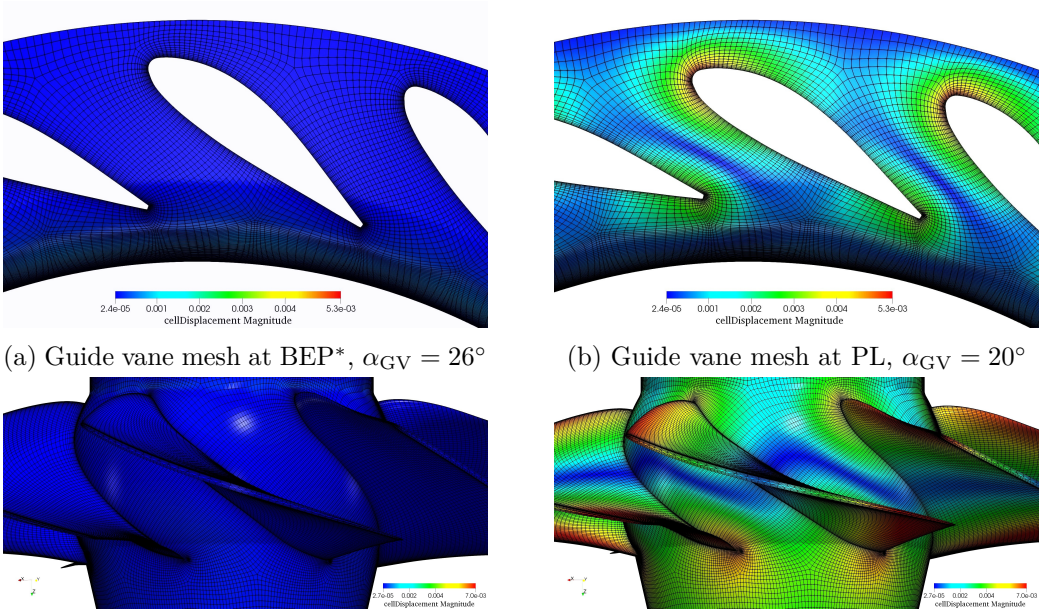

(a) Guide vane mesh at BEP*, $\alpha_{\mathrm{GV}} = 26°$

(b) Guide vane mesh at PL, $\alpha_{\mathrm{GV}} = 20°$

(c) Runner mesh at BEP*, $\alpha_{\mathrm{RB}} = 32.8°$

(d) Runner mesh at PL, $\alpha_{\mathrm{RB}} = 28.8°$

Figure 5: Unmorphed (BEP*) and morphed (PL) meshes of the U9-400 guide vane and runner, colored with contours of the magnitude of the cell displacement field

Two probes, shown in Figure 6, are defined in the present simulation to monitor the pressure variation. The first one is located just before the runner near the hub surface (Probe 1) and the second one is positioned downstream in the draft tube between the center and the wall (Probe 2). In order to calculate the fluctuating part (p') of the pressure signal (p), the instantaneous mean, $\bar{p}$, is needed. $\bar{p}$ is obtained using the Savitzky-Golay finite impulse response filter [11]. Figure 7 presents the variation of pressure, its instantaneous mean, and fluctuations from the instantaneous mean for both the probes during the transient. The static pressure of both the probes indicates an almost constant mean during the stationary BEP* and PL conditions. When the transient is initiated, the Probe 1 pressure starts to decrease. The reduction rate is almost constant since the flow rate and the guide vane and runner blade angles are changing linearly. The fluctuating part of the pressure is larger for Probe 1 than for Probe 2, which is reasonable because it is close to the runner blades. A zoomed view is presented in each figure, showing the data for one runner rotation. It can be seen that the pressure fluctuations at Probe 1 are mostly affected by the Rotor-Stator Interaction (RSI), since the six peaks correspond to the number of runner blades. No obvious dominant frequency is visible at Probe 2.

Fast Fourier Transform (FFT) helps to identify dominant frequencies and their amplitudes. The characteristics of the signal may change in time during the transient procedure. Hence a Short Time Fourier Transform (STFT) analysis should be performed to extract the properties of the fluctuating pressure. Figure 8 depicts the spectrogram of the fluctuating pressure signal

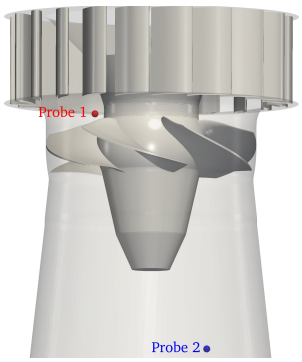

Figure 6: Location of the probes

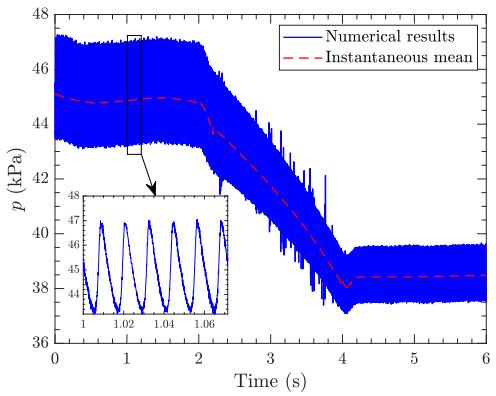

(a) Static pressure for Probe 1

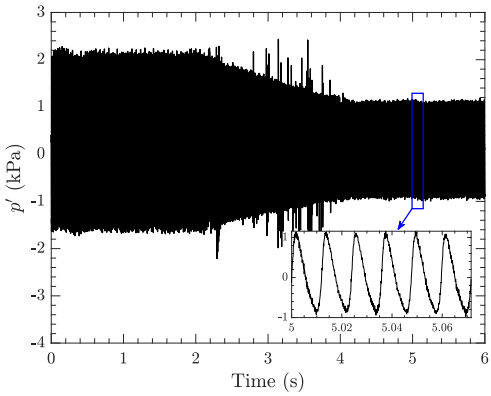

(b) Pressure fluctuations for Probe 1

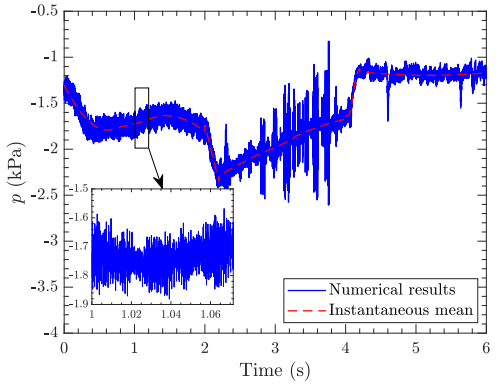

(c) Static pressure for Probe 2

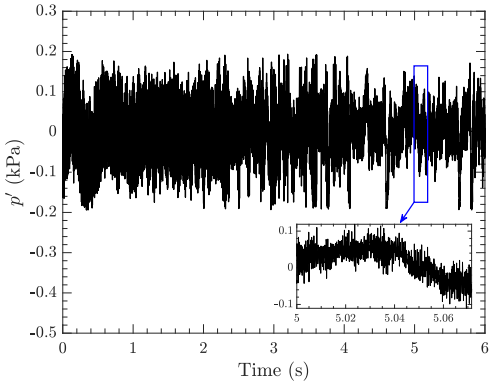

(d) Pressure fluctuations for Probe 2

Figure 7: Static pressure and pressure fluctuations for the two probes during load rejection

for both probes. The vertical axis denotes the frequency normalized with the runner rotation frequency (f_0). The blade and guide vane passing frequencies are defined as

$$f_{\mathrm{b}} = f_0 \cdot Z_{\mathrm{b}} \tag{4}$$

$$f_{\mathrm{gv}} = f_0 \cdot Z_{\mathrm{gv}} \tag{5}$$

where $Z_{\mathrm{b}} = 6$ and $Z_{\mathrm{gv}} = 20$ are the number of runner blades and guide vanes, respectively. It is observed that the runner blade frequency and its harmonics are the dominant frequencies for Probe 1. The guide vane passing frequency is also slightly excited. On the other hand,

the spectrogram of Probe 2, which is located in the draft tube, signifies the dominance of low frequencies due to rotating vortex rope and its breakup.

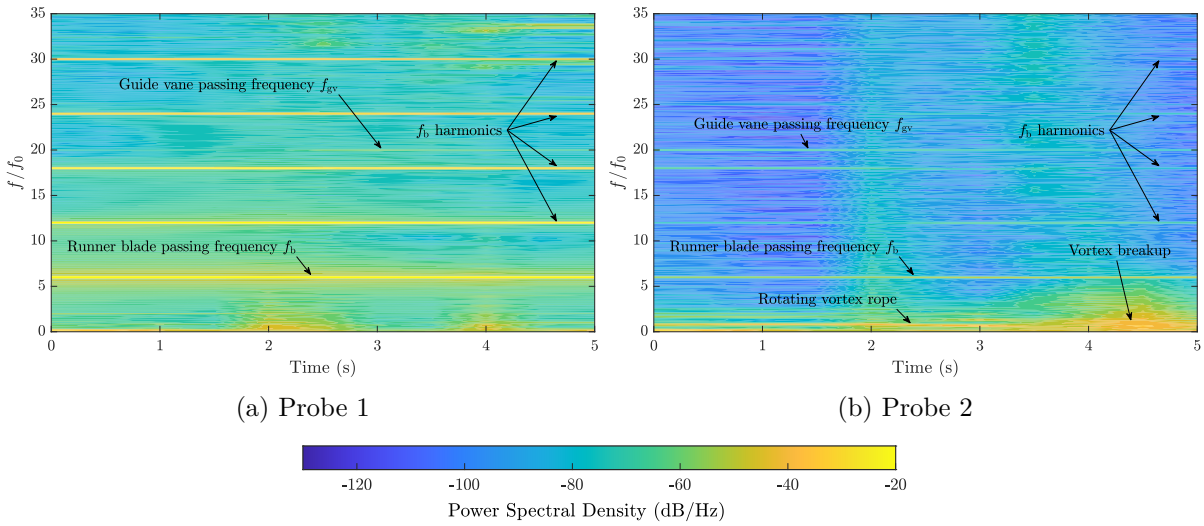

(a) Probe 1 (b) Probe 2

Figure 8: Spectrogram (STFT) of fluctuating pressure signal during load rejection

The λ_2 criterion [12] can be useful to have a better understanding of the flow field structures inside the draft tube during the load rejection procedure. The iso-surfaces of $\lambda_2 = 1000\ \mathrm{s}^{-2}$, colored with velocity magnitude, are shown for both the BEP* and PL conditions in Figure 9. A distinct coherent structure, known as rotating vortex rope, is visible at the BEP* condition. Normally, the turbines are designed so that no vortex rope exists at their BEP condition. This indicates that the assumed BEP* condition for this test case is probably not the real best efficiency point. More numerical and experimental analysis of this new Kaplan turbine model is required to understand the operating conditions. After load reduction, it is seen that vortex rope breaks down and smaller structures are created. Vortical structures created by the runner blade tip clearance and also trailing edge separation are also visible at both BEP* and PL.

5. Conclusion

A novel numerical framework for OpenFOAM is introduced to simulate the flow during transient operation of Kaplan turbines. The conventional mesh deformation methods in OpenFOAM, based on the solution of a Laplacian equation, fails in the Kaplan turbine where the points are supposed to substantially slip on surfaces with high curvatures. The new approach is able to simultaneously rotate the mesh as a solid body, because of runner rotation, and smoothly deform it due to the change of blade angles.

A load rejection transient from BEP* to PL was studied as a test case. Variation of static pressure, its frequencies and amplitudes at different probe locations was studied. It was shown that pressure fluctuations due to rotor-stator interaction and vortex rope breakup can be successfully captured. Finally, the flow structures at the draft tube of the turbine were studied using λ_2 iso-surfaces.

6. Acknowledgements

The research presented was carried out as a part of the “Swedish Hydropower Centre - SVC”. SVC is established by the Swedish Energy Agency, EnergiForsk and Svenska Kraftnät together with Luleå University of Technology, The Royal Institute of Technology, Chalmers University of Technology and Uppsala University, www.svc.nu. The computations were enabled by resources

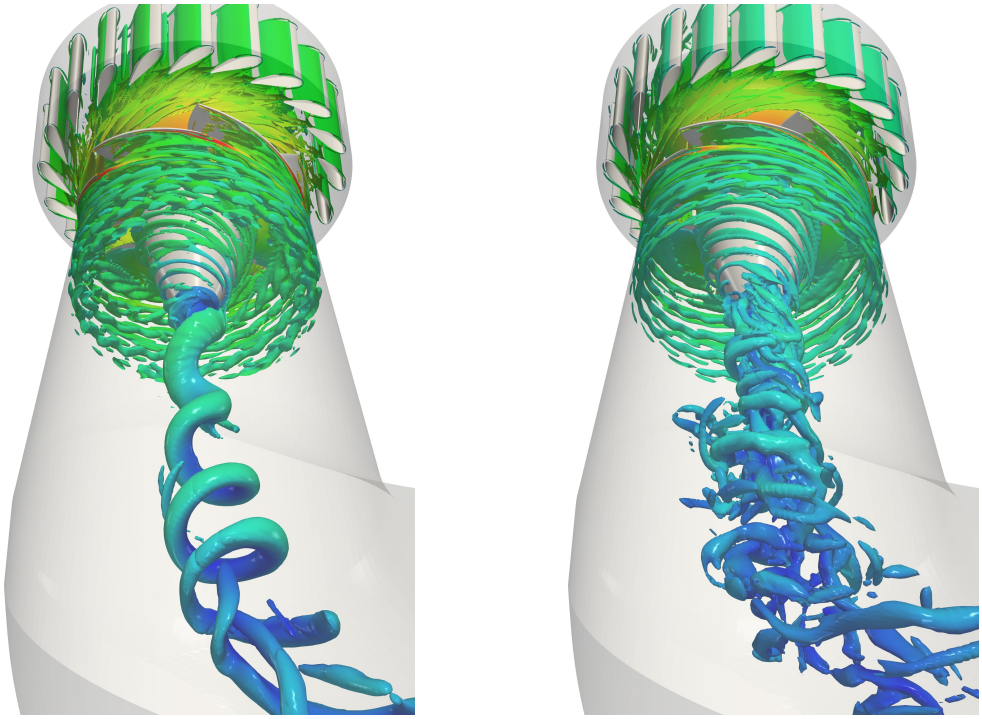

(a) BEP* (b) PL

Figure 9: Visualization of vortical flow structures in the draft tube using iso-surfaces of $\lambda_2 = 1000\ \mathrm{s}^{-2}$

provided by the Swedish National Infrastructure for Computing (SNIC) at NSC partially funded by the Swedish Research Council through grant agreement no. 2018-05973.

References

[1] Goyal R and Gandhi B K 2018 *Renewable Energy* **116** 697 – 709 ISSN 0960-1481
[2] Ferrás L, Nóbrega J and Pinho F 2013 *International Journal for Numerical Methods in Fluids* **72** 724–747
[3] Petit O, Mulu B, Nilsson H and Cervantes M 2010 Comparison of numerical and experimental results of the flow in the u9 kaplan turbine model *25th IAHR Symposium on Hydraulic Machinery and Systems*
[4] Amiri K, Mulu B, Raisee M and Cervantes M 2014 Load variation effects on the pressure fluctuations exerted on a kaplan turbine runner *IOP Conference Series: Earth and Environmental Science* vol 22 (IOP Publishing) p 032005
[5] Mulu B, Cervantes M, Devals C, Vu T and Guibault F 2015 *Engineering Applications of Computational Fluid Mechanics* **9** 139–156
[6] Javadi A and Nilsson H 2017 *International Journal of Heat and Fluid Flow* **63** 1 – 13 ISSN 0142-727X
[7] Egorov Y and Menter F 2008 Development and application of SST-SAS turbulence model in the DESIDER project *Advances in Hybrid RANS-LES Modelling* ed Peng S H and Haase W (Berlin, Heidelberg: Springer Berlin Heidelberg) pp 261–270
[8] Weller H 2012 *Monthly Weather Review* **140** 3220–3234 ISSN 0027-0644
[9] Patankar S and Spalding D 1972 *International Journal of Heat and Mass Transfer* **15** 1787 – 1806 ISSN 0017-9310
[10] Issa R 1986 *Journal of Computational Physics* **62** 40 – 65 ISSN 0021-9991
[11] Savitzky A and Golay M J E 1964 *Analytical Chemistry* **36** 1627–1639
[12] Jeong J and Hussain F 1995 *Journal of Fluid Mechanics* **285** 69–94